

Coordination of physiological traits involved in drought-induced mortality of woody plants

Maurizio Mencuccini^{1,2}, Francesco Minunno³, Yann Salmon¹, Jordi Martínez-Vilalta^{4,5} and Teemu Hölttä³

¹School of GeoSciences, University of Edinburgh, Edinburgh EH9 3FF, UK; ²ICREA at CREAM, Cerdanyola del Vallès, Barcelona 08193, Spain; ³Department of Forest Science, University of Helsinki, PO Box 27, Helsinki FI-00014, Finland; ⁴CREAF, Cerdanyola del Vallès, Barcelona 08193, Spain; ⁵University of Autònoma Barcelona, Cerdanyola del Vallès, Barcelona 08193, Spain

Summary

- Accurate modelling of drought-induced mortality is challenging. A steady-state model is presented integrating xylem and phloem transport, leaf-level gas exchange and plant carbohydrate consumption during drought development.
- A Bayesian analysis of parameter uncertainty based on expert knowledge and a literature review is carried out. The model is tested by combining six data compilations covering 170 species using information on sensitivities of xylem conductivity, stomatal conductance and leaf turgor to water potential.
- The possible modes of plant failure at steady state are identified (i.e. carbon (C) starvation, hydraulic failure and phloem transport failure). Carbon starvation occurs primarily in the parameter space of isohydric stomatal control, whereas hydraulic failure is prevalent in the space of xylem susceptibility to embolism. Relative to C starvation, phloem transport failure occurs under conditions of low sensitivity of photosynthesis and high sensitivity of growth to plant water status.
- These three failure modes are possible extremes along two axes of physiological vulnerabilities, one characterized by the balance of water supply and demand and the other by the balance between carbohydrate sources and sinks. Because the expression of physiological vulnerabilities is coordinated, we argue that different failure modes should occur with roughly equal likelihood, consistent with predictions using optimality theory.

Author for correspondence:

Maurizio Mencuccini

Tel: +44 131 6505432

Email: m.mencuccini@ed.ac.uk

Received: 22 January 2015

Accepted: 11 April 2015

New Phytologist (2015) **208**: 396–409

doi: 10.1111/nph.13461

Key words: drought-induced mortality, optimality, phloem transport, phloem viscosity, photosynthetic down-regulation, source–sink relationships, water stress, xylem embolism.

Introduction

Mortality of plants as a consequence of drought events has become a major focus of attention recently, as a result of reports highlighting severe mortality episodes around the globe (e.g. Allen *et al.*, 2010; Peng *et al.*, 2011). Current process-based models do not adequately represent local and regional mortality, because they have been constructed primarily to represent the fluxes of carbon (C), water and nutrients and because they have not been calibrated against datasets of severe drought episodes (McDowell *et al.*, 2013; Powell *et al.*, 2013). Consequently, doubts exist as to their capacity to predict shifts in vegetation composition as a consequence of increased drought frequency and intensity (e.g. Anderegg *et al.*, 2012; Adams *et al.*, 2013; Xu *et al.*, 2013; Meir *et al.*, 2015).

One central element of uncertainty is given by the lack of detailed understanding of the environmental, ecological and physiological processes leading to mortality (McDowell *et al.*, 2013). The existing datasets that have documented plant mortality paying sufficient attention to some of the underlying physiology (e.g. Adams *et al.*, 2009; Fisher *et al.*, 2010; Anderegg *et al.*, 2012; Hartmann *et al.*, 2013; Mitchell *et al.*, 2013; Poyatos *et al.*,

2013) differ in the emphasis given to different aspects of the mortality process. Partly as a consequence, different interpretations of the main processes affecting mortality have emerged (McDowell *et al.*, 2008; Adams *et al.*, 2009; Sala, 2009; McDowell & Sevanto, 2010; Sala *et al.*, 2010). In addition, biotic interactions can interact significantly with the physiological status of the plants to increase the chances of drought-related mortality (Dobbertin & Rigling, 2006; Wermelinger *et al.*, 2008; Galiano *et al.*, 2011; Heiniger *et al.*, 2011; McDowell, 2011; Krams *et al.*, 2012; Zweifel *et al.*, 2012; McDowell *et al.*, 2013).

Being able to avoid death is arguably the most important attribute that living organisms must possess to reach reproductive age and transmit their genes to future generations. A tenable assumption is that, over evolutionary times, plants have adopted strategies that minimize their chances of failing quickly in response to multiple abiotic hazards such as drought (e.g. Anderegg *et al.*, 2013). From this perspective, the threats of mortality caused by failure of the hydraulic transport systems (xylem or phloem) and of starvation caused by lack of C can be viewed as possible extremes across a continuum of physiological vulnerabilities (Meir *et al.*, 2015). From an evolutionary perspective, the expression of functional traits might be optimally coordinated to

minimize the chance that any one source of mortality risk prevails. If that was not the case, plants would arguably be over-built with respect to the risk posed by individual hazards.

The present work has three main objectives. First, we present a steady-state model that incorporates many of the processes involved in drought-induced mortality, with an emphasis on the interaction between water and C fluxes. In the framework proposed by McDowell *et al.* (2008), the central distinction is between length and intensity of drought events, mediated by the degree of isohydric regulation of water potential. Here, we expand that analysis. Second, we explore the biological parameter space of the model, which constrains the range of water- and C-related processes leading to physiological failure and mortality. Finally, we employ empirical data to test the optimality idea set out earlier, that mortality risks should be equally likely across a broad spectrum of species, thanks to the coordination of the relevant functional traits. A steady-state model has distinct advantages compared with time-dependent approaches, because assumptions about poorly known processes (such as thresholds and regulatory dynamics of carbohydrate pools) are avoided and because the number of parameters is small enough that fitting to empirical datasets with quantified uncertainty is possible (Meir *et al.*, 2015). It suits our objective to determine the trait set involved in mortality, rather than predicting the time courses to death.

Description

Model structure

The steady-state model develops a previously published coupled xylem and phloem transport model (Hölttä *et al.*, 2009a).

Definitions, symbols, units and choice of values for all the parameters employed in the model are given in Tables 1 and 2 (for the parameters whose values were changed and those that were kept fixed, respectively). A diagrammatic representation of model structure is given in Fig. 1, with the represented processes individually numbered. In the two parallel transport systems of the xylem and the phloem, axial hydraulic conductances of all vertical elements are calculated from cross-sectional areas and hydraulic conductivities. Following Minunno *et al.* (2013), we determined the number of finite elements required to resolve the system's nonlinear responses. We progressively shortened the number of elements of the catena from 100 to 10. For all state variables, the difference in outputs between catenas with 100 and 40 elements was very small. The difference in outputs between catenas with 40 and 10 elements was generally < 5%. The final simulations were carried out with 100 elements.

The xylem water pressure at each element is calculated from the water pressure of the element underneath it (for the bottom-most element of the catena, this is the soil water potential, Ψ_{soil} in Fig. 1) minus the effects of gravity and the viscous pressure losses caused by xylem sap flux (F_{xyl} in Fig. 1). For each vertical phloem element, equations of radial water exchange with the xylem (F_{radial} in Fig. 1), phloem axial sap flow (F_{ph} in Fig. 1), water conservation and solute conservation are written (Hölttä *et al.*, 2009a). The boundary condition at the bottom-most element of the phloem (the 'sink') is such that the sugar unloading rate at the sink maintains a 'target' turgor pressure (U_{100} in Fig. 1). Different values of this target turgor pressure were employed, with their range given in Supporting Information Fig. S1(A). The viscosity of the phloem sap is a function of its sucrose concentration at each element using an equation describing this

Table 1 The 11 parameters employed to explore the sensitivity of model structure to the various modes of plant failure to drought

Parameter	Symbol	Units	50% percentile	2.5% and 97.5% percentiles of the distribution sampled
Maximum xylem hydraulic conductance	K_x	$\text{m}^3 \text{MPa}^{-1} \text{s}^{-1}$	2.42×10^{-6}	2.21×10^{-7} 3.68×10^{-5}
Maximum phloem hydraulic conductance	K_{ph}	$\text{m}^3 \text{MPa}^{-1} \text{s}^{-1}$	1.69×10^{-4}	1.86×10^{-5} 1.58×10^{-3}
Water potential Ψ causing 50% loss of K_{xyl}	B_x	MPa	-3.69	-14.38 -1.21
Water potential Ψ causing 50% loss of g_s	B_{gs}	MPa	-0.79	-12.21 -0.11
Maximum photosynthesis	P_{max}	mol s^{-1}	6.62×10^{-5}	6.72×10^{-6} 6.02×10^{-4}
Leaf osmotic pressure at which P goes to zero	c_{max}	MPa	9.24	2.18 60.19
Base respiration rate	R_0	mol s^{-1}	3.36×10^{-6}	1.61×10^{-7} 6.05×10^{-5}
Osmotic pressure above which R begins to increase as a function of c	c_{min}	MPa	1.46	0.22 10.78
Slope of the xylem vulnerability curve	A_x	% PLC MPa^{-1}	2.25	0.11 3.43
Slope of relationship between stomatal conductance and water potential Ψ	A_{gs}	% closure MPa^{-1}	8.09	1.34 30.52
Turgor pressure at the bottom of the phloem	U	MPa	0.63	0.09 3.43

Each parameter is defined, the symbol and the units are given, as well as the central value employed in the simulations and the range of values sampled.

Table 2 The six parameters of the model which were kept fixed in the simulations carried out to explore the sensitivity of model structure to the various modes of plant failure to drought. Each parameter is defined, the symbol and the units are given, as well as the fixed value employed in the simulations

Parameter	Symbol	Units	Central value
Tree height	h	m	10
Phloem cross-sectional area	A_p	m ²	1.2×10^{-4}
Xylem cross-sectional area	A_x	m ²	2×10^{-3}
Xylem–phloem radial conductance	K_{rad}	m ³ Pa ⁻¹ s ⁻¹	2×10^{-11}
Transpiration rate at full stomatal opening	T_0	m ³ s ⁻¹	2.25×10^{-6}
Slope of the photosynthetic response curve to stomatal conductance	γ	–	0.2

dependency accurately up to osmotic potentials of *c.* –8 MPa (see Morison, 2002 and the green dashed double-headed link in Fig. 1 linking phloem sucrose osmotic potential, c_{ph} , with phloem conductance, K_{ph}). This is an essential feature of the Hölttä *et al.* (2009a) model resulting from sucrose being the only solute transported and also the cause for the increases in viscosity. It predicts a point of potential vulnerability for the phloem if the system fails to transport all the products of photosynthesis. A very dilute solution minimizes viscosity but requires large volume fluxes, while a very concentrated solution minimizes volume fluxes but increases viscosity. Jensen *et al.* (2013) showed that this problem leads to an optimal solute concentration that is broadly consistent with the concentrations normally measured in plants under well-watered conditions (see Lang (1978) and Hölttä *et al.* (2009a), for similar arguments). In practice, it translates into a vulnerability curve for the phloem as a function of phloem osmotic potential (Fig. S1(B)) for consistency with the citation of other panels of Fig. S1, equivalent to the one for the xylem as a function of xylem water potential. The two main parameters

affecting the shape of this phloem vulnerability curve are maximum phloem hydraulic conductance and the type of transported osmoticum.

Simulations are driven only by soil water potential (MPa), while transpiration and photosynthesis do not depend on other environmental variables. For each value of soil water potential, a steady-state solution is first found for the xylem water potential profile, percentage loss of hydraulic conductivity (PLC) and stomatal conductance, by iterating Eqns 1–5 (see later) plus Darcy's law, until water potential of the uppermost element varies by <0.001 MPa. The procedure is repeated to find steady-state values of phloem transport rates, photosynthesis and respiration, following an approach similar to the one presented in Hölttä *et al.* (2009a). The model normally converges very quickly and 500 000 runs take a few hours on a desktop computer.

Xylem vulnerability to cavitation

For each element *i* of the catena, xylem conductance decreases with decreasing water potential according to Pammenter & Vander Willigen (1998):

$$k_x = k_{0,x}(1 - PLC_i) \quad \text{Eqn 1}$$

where

$$PLC = \frac{1}{(1 + \exp(A_x(\Psi - B_x)))} \quad \text{Eqn 2}$$

In Eqn 2, Ψ is 'xylem' water potential at any point in the catena and the parameter B_x can be interpreted as the water potential at which xylem conductance reaches 50% of its maximum value (referred to as P50; Pammenter & Vander Willigen, 1998). Parameter A_x represents instead the slope of the

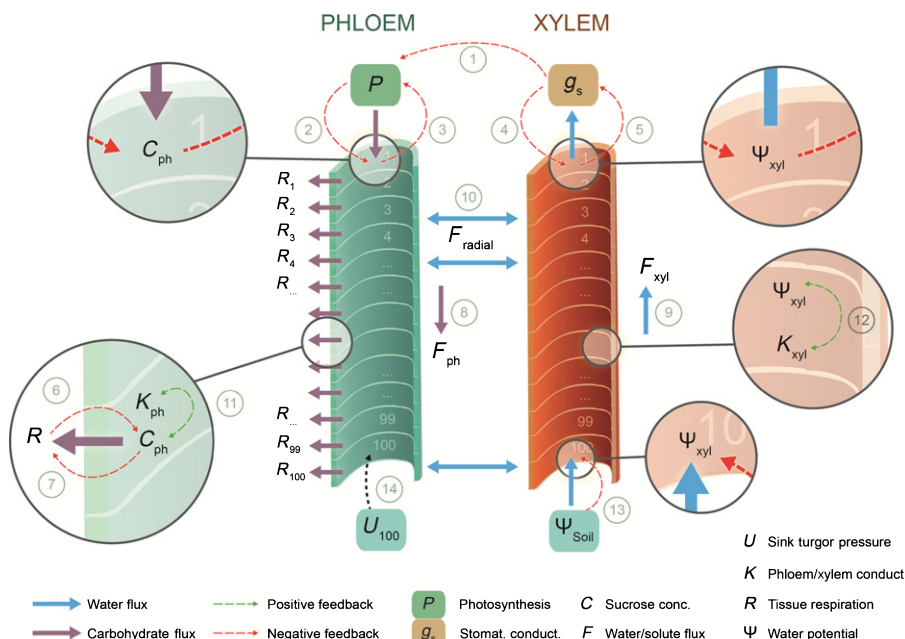


Fig. 1 Diagrammatic representation of model structure. The two central open tubes indicate xylem and phloem transport (brown and green, respectively). *P*, photosynthesis; *g_s*, stomatal conductance; *R*, respiration, *F_{ph}*, *F_{radial}* and *F_{xyl}*, phloem, radial and xylem transport rates, respectively; *c_{ph}*, phloem osmotic pressure; *U₁₀₀*, turgor pressure in unloading element; *K_{ph}* and *K_{xyl}*, phloem and xylem conductance; Ψ_{soil} and Ψ_{xyl} , soil and xylem water potential, respectively. Numbers 1–100 inside the green (phloem) tube for *R* refer to the corresponding finite elements of the numerical model. Each of the blown-up circles represents one or more processes or feedbacks that are incorporated in the model. The progressive numbers from 1 to 14 inside the grey circles refer to the 14 processes represented in the model and discussed in the text.

relationship, that is, the gradient of change in PLC with changes in water potential. It has been shown (Cochard, 2006; Choat *et al.*, 2012) that these two parameters are related, that is, plants with vulnerable xylem (i.e. high B_x) also have steep vulnerability curves (high A_x) and vice versa. Two examples of curves drawn with extreme values of A_x and B_x taken from the sampled distribution are given in Fig. S1(C). Beyond its sensitivity to xylem water potential, plant conductance in Eqn 1 also depends strongly on the value of maximum hydraulic conductance, $K_{0,x}$.

Transpiration rate and stomatal conductance

Transpiration rate is represented as (e.g. Jarvis & McNaughton, 1986):

$$T = g_s T_0 \quad \text{Eqn 3}$$

The maximum transpiration rate, T_0 , is given a fixed value of $2.25 \times 10^{-6} \text{ m}^3 \text{ s}^{-1}$ (i.e. 50 mmol $\text{m}^{-2} \text{ s}^{-1}$ for a 25 m^2 tree) and the parameter space of suitable hydraulic values is varied by changing the maximum plant hydraulic conductance, $K_{0,x}$. Fig. S1(D) shows how the two most extreme values of the parameter $K_{0,x}$ coupled with T_0 affect plant water potentials, following Darcy's law.

While water flux affects xylem Ψ , leaf Ψ affects stomatal conductance, g_s , reducing the chances of extremely low water potentials. Similarly to the case for xylem hydraulic conductance, stomatal conductance declines with plant water potential following a sigmoidal curve:

$$g_s = g_{s,0} (1 - \text{PLC}_{g_s}) \quad \text{Eqn 4}$$

and

$$\text{PLC}_{g_s} = \frac{1}{(1 + \exp(A_{g_s}(\Psi - B_{g_s})))} \quad \text{Eqn 5}$$

where $g_{s,0}$ is set to 1.00 and g_s is constrained to vary in the range $0 \leq g_s \leq 1$ in Eqns 3 and 4. In Eqn 5, Ψ is 'leaf' (the top element of the catena) water potential and the parameter B_{g_s} can also be interpreted as the leaf water potential at which stomatal conductance reaches 50% of its maximum value (see Tuzet *et al.* (2003) for a representation of the relationship between photosynthesis and stomatal conductance that responds to leaf Ψ). Two extreme examples of the relationship employed here are given in Fig. S1 (E).

Photosynthesis rate

Photosynthesis rate is modelled as (Mäkelä *et al.*, 1996):

$$P = P_{\max} \frac{g_s}{g_s + \gamma} f_{\text{ns}} \quad \text{Eqn 6}$$

where P_{\max} is a parameter setting the maximum photosynthesis rate, g_s is the stomatal conductance (in relative units from

0 to 1), γ is a parameter describing the saturation of photosynthesis with respect to stomatal opening, and f_{ns} is a factor accounting for the down-regulation of photosynthesis as a function of the osmotic pressure at the source (not included in Mäkelä *et al.*, 1996). Albeit empirical (see von Caemmerer & Farquhar, 1981), Eqn 6 incorporates the effects of stomatal aperture and of sink regulation of photosynthesis (e.g. Paul & Foyer, 2001). In a preliminary analysis, we let the parameter γ vary, but found that its effect on output variables was very small. We therefore kept it fixed in all analyses at a value of 0.2.

Because photosynthesis occurs at the top of the catena of phloem transport cells (the 'source') and sucrose is assumed to be loaded directly into the phloem, f_{ns} is dependent on the sucrose osmotic pressure of the first phloem cell c_1 at the top of the catena (where c_1 is in MPa). The effect of progressive concentration of the products of photosynthesis is therefore represented as:

$$f_{\text{ns}} = \frac{c_{\max} - c_1}{c_{\max}} = 1 - \frac{c_1}{c_{\max}} \quad \text{Eqn 7}$$

where c_{\max} is the parameter giving the maximum osmotic pressure of the phloem (MPa). If $c_1 = 0$, there is no down-regulation ($f_{\text{ns}} = 1$); if $c_1 = c_{\max}$, photosynthesis is depressed to zero ($f_{\text{ns}} = 0$) to avoid further phloem loading. Fig. S1(F) gives a representation of this relationship using the two extreme values of P_{\max} and c_{\max} employed. Because of our steady-state assumption, photosynthesis rates and phloem loading rates are equal, unless the plant fails. In additional model runs, we compared this model against a representation of the down-regulation of photosynthesis by leaf water potential using the following formulation for f_{ns} :

$$f_{\text{ns}} = \exp(P_{\text{mod}} \Psi) \quad \text{Eqn 8}$$

where P_{mod} ($P_{\text{mod}} > 0$) is the parameter setting the direct sensitivity of P_{\max} to leaf water potential.

Growth and respiration

Growth and growth respiration are not explicitly separated from maintenance respiration, but we assume that the substrate is partially consumed during its transit along the phloem catena (e.g. Dewar, 1993; Cannell & Thornley, 2000). This approach is similar to the idea that 'source' photosynthesis and 'sink' respiration are colimiting processes, resulting in a near-homeostasis of phloem solute osmotic potential profiles as drought develops (i.e. Thornley & Johnson, 1990; Minchin *et al.*, 1993; Farrar, 1996; Minchin & Thorpe, 1996; Bijlsma & Lambers, 2000; Bancal & Soltani, 2002).

The respiration rate, R , from each element i along the catena of phloem transport is assumed to be constant for values of the osmotic pressure, c_i , between 0 and c_{\min} . Above c_{\min} (i.e. for more positive osmotic pressures than c_{\min}), R increases linearly as a function of c_i . Therefore:

$$R_i = R_0 = 0.10 \frac{P_{\max}}{N} \quad \text{Eqn 9}$$

$$R_i = R_0 \frac{c_i}{c_{\min}}$$

for $c_i \leq c_{\min}$ and $c_i > c_{\min}$, respectively (Fig. S1G). R_0 is the base respiration rate at minimum substrate availability. The central value of R_0 was set at 10% of P_{\max} divided by N , the number of elements of the catena. Uncertainty in this parameter was introduced by Monte-Carlo sampling of the parameter space (see later). In the baseline scenario, we assumed no direct dependency of respiration on plant water status. In additional simulations (see Table S3), a direct dependency of respiration on water potential was introduced using a different formulation, as done earlier for P_{\max} , that is,

$$R_i = R_0 \exp(R_{\text{mod}} \Psi) \quad \text{Eqn 10}$$

where R_{mod} ($R_{\text{mod}} > 0$) is the parameter setting the direct sensitivity of R_0 to water potential.

In the baseline simulations, increased phloem concentrations during drought always lead to increased respiratory losses (cf. Eqn 9). The dependency on water potential of Eqn 10, either alone or in combination with Eqn 9, allows for the moderating effects of low plant water status on plant respiration when phloem concentrations are high.

Because we assumed a constant sink turgor pressure (see earlier), each solution for steady-state photosynthesis and respiration resulted in a certain amount of carbohydrates not being employed for respiration and being unloaded at the sink. We refer to this fraction as F_{resid} , the residual flux of transported carbohydrates. This metric is useful as an indicator of carbohydrate availability or potential carbohydrate storage, as it represents the fraction produced in the leaves, transported through the phloem, not respired by the catena and unloaded at the sink.

Definition of modes of failure

Some of the processes represented in the model contain negative feedback loops that tend to stabilize plant performance and avoid runaway failure (red arrows in Fig. 1). Two of the processes (drought-induced cavitation in the xylem and viscosity-induced reductions of conductance in the phloem; green arrows in Fig. 1) are destabilizing feedback loops that can lead to failure. We classified the possible modes of plant failure at steady state as:

(1) Hydraulic failure (HF). A combination of parameters was assumed to lead to HF when the calculated rate of xylem hydraulic conductance fell to zero as a result of complete xylem cavitation, that is,

$$K_x = 0 \quad \text{Eqn 11}$$

(2) Carbon starvation (CS). A combination of parameters was assumed to lead to CS when the calculated steady-state rate of photosynthesis was lower than the steady-state rate of respiration by the catena, that is,

$$P < R_{\text{tot}} \quad \text{Eqn 12}$$

Because respiration was calculated for each element of the model separately, R_{tot} represents the sum of the N respiratory terms. By definition, $F_{\text{resid}} = 0$ when $P \leq R_{\text{tot}}$.

(3) Phloem transport failure (PF). A combination of parameters was assumed to lead to PF when the rate of photosynthesis was greater than the rate at which carbohydrates could be transported out of the leaf as a result of excess phloem viscosity, that is,

$$F_{\text{ph}} < P \quad \text{Eqn 13}$$

The definitions of such modes of failure need to be interpreted in the narrow sense that is consistent with the use of a steady-state model, as opposed to the broader definitions applicable to the field. For example, the definition of CS should be relaxed to the broader negative C balance under prolonged nonsteady-state conditions, because a negative C balance during a short time period does not necessarily lead to failure. Similarly, the narrow criterion of PF for steady-state conditions should be relaxed to the broader lack of equilibrium between photosynthesis and phloem transport (and therefore changing storage pools) under nonsteady-state conditions.

Exploration of parameter space

Of the 17 model parameters, 11 have the potential to affect the likelihood and the mode of plant failure. The behaviour of 11 of these parameters (13 including P_{mod} and R_{mod}) was examined by carrying out a prior parameter uncertainty quantification (van Oijen *et al.*, 2013) to determine the sensitivity of model outputs to uncertainty in the global parameter space, as opposed to changes in individual parameters (i.e. Beven & Binley, 1992). We defined the prior parameter space based on literature estimates. We examined compilations that summarized hydraulic traits for different biomes and plant functional types (see Notes S1). For each compilation, we extracted the range of the main hydraulic parameters to set the limits of our prior distributions. Values of maximum photosynthetic rates were constrained based on values from the GLOPNET database (Wright *et al.*, 2005).

We used log-normal distributions for our sampled parameter space (Table 1 and Hölttä *et al.*, 2009a), with 95% of the values within limits obtained by multiplying and dividing the central estimate by 10. Parameters were generally sampled using univariate log-normals. Multivariate log-normals were sampled using the function `mvnorm` in the library MASS (Venables & Ripley, 2002) in R 3.0.2 (R Development Core Team, 2013) for the parameters related to xylem vulnerability curves and for those related to the response of stomatal conductance to water potential. For the first set of parameters (i.e. A_x and B_x and K_x), the covariances ensured that A_x and B_x were positively and curvilinearly related (Cochar, 2006; Choat *et al.*, 2012) and that high values of B_x (i.e. values of P50 close to zero) loosely corresponded to high values of xylem K . For the second set of parameters, the covariance ensured that A_{gs} and B_{gs} were similarly positively but loosely related (Manzoni *et al.*, 2013, 2014).

Sampling was repeated 500 000 times. For each of the 500 000 parameter combinations, a drought sequence was imposed on the model plant, starting from a soil water potential of -0.005 MPa and continuing in steps of 0.005 MPa. At each step, the model calculated the steady-state values of all state variables and checked whether the three conditions defining the modes of failure (Eqns 11–13) were encountered. If steady-state values could be found for all state variables and none of those conditions were satisfied (i.e. if $P = F_{\text{ph}} > R_{\text{tor}}$ and $K_{\text{xy1}} > 0$), the soil water potential was lowered. This process continued until a value of soil water potential was reached at which one of these conditions was satisfied. At this point, failure was deemed to have been reached as CS, HF or PF.

The 500 000 combinations of initial parameter values, output variables and classified modes of failure were screened to eliminate runs that were clearly outside the range of realistic values ('nonbehavioural simulations'; Beven & Binley, 1992). This was accomplished by selecting limits to two variables, that is, leaf water potential and water-use efficiency. Runs were given a probability of 1 only if: (a) steady-state values of 'leaf' water potentials Ψ at a soil water potential of -0.005 MPa were within the range $-3.0 < \Psi < -0.2$ Mpa; and (b) the internal water-use efficiency (i.e. the ratio of assimilation divided by stomatal conductance) did not decrease between the soil water potential of -0.005 MPa and the critical soil water potential at failure. Alternatively, runs were given a probability of 0. Condition (a) ensured a loose coupling between transpiration rate T and xylem hydraulic conductance, forcing realistic values of water potentials. Condition (b) ensured that those parameter combinations resulting in reductions in internal water-use efficiency during a drought (e.g. caused by a combination of stomatal conductance being very insensitive to leaf water potential and photosynthesis rate being very sensitive to calculated sucrose concentrations or leaf water potential) were excluded.

Model sensitivity analyses

To determine the sensitivity of model outputs to input parameters, we conducted a canonical correlation analysis (CCA, Hair *et al.*, 1998). CCA is a multivariate technique allowing the study of the relationships among sets of correlated multiple dependent (model outputs) and independent variables (model parameters; see Notes S1, Table S2). In addition, we determined the sensitivity of the frequency distributions of the three failure modes to the model boundary conditions and carried out additional simulations varying model parameters that were kept fixed for all the other runs (i.e. phloem radial hydraulic conductance, tree height, degree and direction of correlations between stomatal and xylem parameters). Finally, we compared these results with those obtained after introducing a direct dependency of basal respiration rate and/or maximum photosynthetic rate on plant water potential.

Empirical data analysis

To analyse model behaviour, we used studies that reported values of the sensitivity of xylem conductivity to Ψ , of stomatal

conductance to leaf Ψ , and of leaf turgor to Ψ (Bartlett *et al.*, 2012; Choat *et al.*, 2012; Manzoni *et al.*, 2013, 2014; Klein, 2014; Nardini & Luglio, 2014). Six additional species came from Vilagrosa *et al.* (2014). The P50 values given by Choat *et al.* (2012), Vilagrosa *et al.* (2014), Klein (2014) and Manzoni *et al.* (2013) were directly equated with B_x . Manzoni *et al.* (2013) and Klein (2014) directly reported B_{gs} , using stomatal conductance and sap flux data against leaf Ψ . A significant overlap in the species coverage of these two datasets was found, even though absolute values of B_{gs} were frequently different between them. The Manzoni *et al.* (2014) dataset is an expanded version of the Manzoni *et al.* (2013) version. Bartlett *et al.* (2012), Nardini & Luglio (2014) and Vilagrosa *et al.* (2014) reported Ψ_{t1p} (water potential at turgor loss point, that is, the Ψ at which leaves, on average, lose turgor). Ψ_{t1p} is an index of plant resistance to water stress and does not directly control the dependency of stomatal conductance to water potential. Estimates of B_{gs} obtained from the relationship between sap flux data and water potentials have similar limitations. Values of Ψ_{t1p} were only assumed to be proportional to B_{gs} and the assumption of proportionality between Ψ_{t1p} to B_{gs} was tested in three ways. First, we let the proportionality coefficient between Ψ_{t1p} and B_{gs} vary between 0.3 and 1.0 and we checked whether changes in these coefficients affected our conclusion on the distribution of species values in model parameter space (see Notes S2, Tables S4, S5, and Figs S2, S3). Second, we checked databases for species with pairs of values of B_{gs} and Ψ_{t1p} . We found 14 species, giving a correlation coefficient of 0.57 ($P < 0.05$), confirming that a relationship between the two estimates can be postulated. Third, to avoid systematic biases, we employed additional categorical variables ('dataset' and 'method'), to test the effects of the individual datasets and of the two methods employed to calculate B_{gs} . We crossed these seven data-sets for common species, checked nomenclature, standardized definitions for biome and eliminated duplications for individual species by value-averaging. Plants were separated into the groups of angiosperms and gymnosperms. Coupled values of B_x and B_{gs} were found for 243 independent observations and 170 species across all compilations. The relationship between B_x and B_{gs} was tested using a general linear model in R 3.0.2 (R Development Core Team, 2013), using 'dataset', 'biome' and 'plant group' as additional categorical factors.

Results

Sensitivity analyses and distributions of simulations by failure modes

The boundary conditions selecting the 'behavioural' simulations screened out a significant number of parameter combinations (92% in the baseline case). Of the simulations that were retained under the baseline case, 25% resulted in HF, 71% in CS and only 4% in PF. These proportions varied greatly (see Table S3) depending on the imposed boundary conditions, especially tree height (varied between 1 and 100 m) and radial hydraulic conductance (varied between 2×10^{-13} and 2×10^{-9}). The parameter that most affected the frequency distributions of the failure

modes was the dependency of plant respiration on water potential. Including this additional parameter (which varied from 0.1×10^{-6} to 1×10^{-6}) increased the proportion of HF (from generally $< 20\%$ to $> 30\%$) and PF (from *c.* 5% to $> 10\%$) at the expense of CS (from $> 75\%$ to $< 60\%$).

Model output variables showed sensitivity to a range of parameters for the first five canonical variates (cf, Table S2 in Notes S1). Two parameters with opposing effects (i.e. xylem K and the slope of the stomatal response to Ψ) affected almost the entire set of output variables. Plant failure mode was primarily related to xylem K , the slope of the stomatal response to Ψ and both xylem and stomatal P50.

Distribution of parameters

The general distribution of the input parameters by mode of failure is given in Fig. 2. The last columns (in red) are the reference empirical distributions for those parameters for which data were available from the meta-analyses. In general, the distributions obtained for the three failure modes (in black) encompassed the distributions from the empirical compilations (in red). Xylem conductance K_x showed a significant difference ($P < 0.001$) in the parameter distribution between the three modes of failure, with higher values for PF than CS. An even more accentuated difference was found for B_x (xylem P50) and A_x , with much higher values found for mode HF, followed by CS and PF ($P < 0.001$). Conversely, B_{gs} (stomatal P50) and A_{gs} showed higher values for CS ($P < 0.001$), with no difference between HF and PF. PF was characterized by a combination of parameter distributions, that is, relatively high K_x , low B_x and A_x (both $P < 0.001$), large c_{max} ($P < 0.001$) and relatively higher c_{min} and sink turgor U . The distributions of the input parameters by mode of failure did not vary by varying the boundary parameters in the sensitivity analysis (data not shown).

The distribution of the main output variables at failure showed (Fig. 3) that soil and leaf Ψ varied across modes of failure, with significantly more negative values for PF ($P < 0.001$). This was associated with higher source turgor pressures ($P < 0.001$), more negative osmotic potentials (in turquoise, $P < 0.001$, as expected for PF by viscosity) and larger turgor drops from leaves to sink ($P < 0.001$). Parameter combinations that resulted in HF showed 100% loss of xylem conductance (in turquoise), almost complete stomatal closure and no photosynthesis. Relative to PF, CS was characterized by lower photosynthetic rates at failure (but not by higher cumulative respiration) and lower cumulative residual fraction of transported carbohydrates at the sink (in turquoise, as expected for this mode of failure). The range of soil water potentials at failure did not differ between HF and CS. The distributions of the output variables at failure varied only marginally by varying the boundary parameters (data not shown).

Controls on modes of failure

A plot of xylem P50 vs stomatal P50 separated HF vs CS (Fig. 4). HF was characterized by points distributed at the top of the space

delimited by B_x (xylem P50), whereas CS was characterized by points distributed on the side of the parameter space characterized by high values of B_{gs} (stomatal P50). Around a diagonal space from top right to bottom left (i.e. from sensitive stomata plus vulnerable xylem to insensitive stomata plus resistant xylem), a relatively wide region of overlap between the two modes of failure was found. Fewer points were found in the left bottom corner of the parameter space. For each of the two modes of failure, plant water potential at failure depended on parameter combinations. Low (negative) values of xylem P50 resulted in low critical leaf water potentials for the case of HF. Similarly, for the case of CS, low values of stomatal P50 resulted in low critical leaf water potentials.

When the 170 species from the meta-analytical compilations were plotted on the $B_x - B_{gs}$ space (as in Fig. 4), the vast majority of the points fell within a region covering the bivariate 99% ranges of these two modes of failure around the main diagonal line (Fig. 5). A significant positive relationship was found between xylem P50 and stomatal P50 across all datasets (all $P < 0.001$, depending on the assumed relationship between stomatal turgor loss point and B_{gs} ; see Table 3 and Tables S4, S5 in Notes S2), with a significant negative intercept for the gymnosperms ($P < 0.001$), indicating a lower P50 (between *c.* -1.1 and -1.9 MPa) for a fixed stomatal P50. Highly significant effects were also found for 'dataset' (with significant differences for the *Vilagrosa* dataset, $P < 0.001$) and 'biome' (with significant differences for the dry sclerophyllous biome, $P < 0.001$). The overall model, including stomatal P50, the three categorical variables and their interactions, explained between 59 and 60% of the variance (Table 3, S4, S5). Despite changes in the distribution and linear fits in Fig. 5 depending on the assumption made for the conversion between leaf stomatal P50 and Ψ_{tlp} , the bulk of the data points remained in the area of joint overlap between the two bivariate distributions of 99% of the simulations for HF and CS (Figs S2, S3 in Notes S2).

Carbon starvation and PF differed for parameter combinations regulating plant C source-sink balance. Because multiple parameters affected the photosynthetic and respiratory responses, composite response parameters were calculated for each, following the response curves given in Eqns 9-13. Relative to PF, CS was characterized by parameter combinations leading to a weak regulation of respiration ($-R_0/Uc_{min}$, that is, base respiration; degree of respiration down-regulation by osmotic pressure and phloem turgor pressure; see Fig. 2) and a strong regulation of photosynthesis ($P_{max} B_{gs}/c_{max}$, i.e. maximum photosynthesis, water potential at 50% loss of stomatal conductance and photosynthetic down-regulation by osmotic pressure) in response to water stress (Fig. 6a). Conversely, for PF, the combination of parameters regulating C fixation, phloem transport and respiration during drought led to a less sensitive regulation of C losses and to a more sensitive regulation of the sinks (Fig. 6b). This resulted in combinations leading to PF being situated above the line of C supply/demand and those leading to CS being situated below or on it (Fig. 6b).

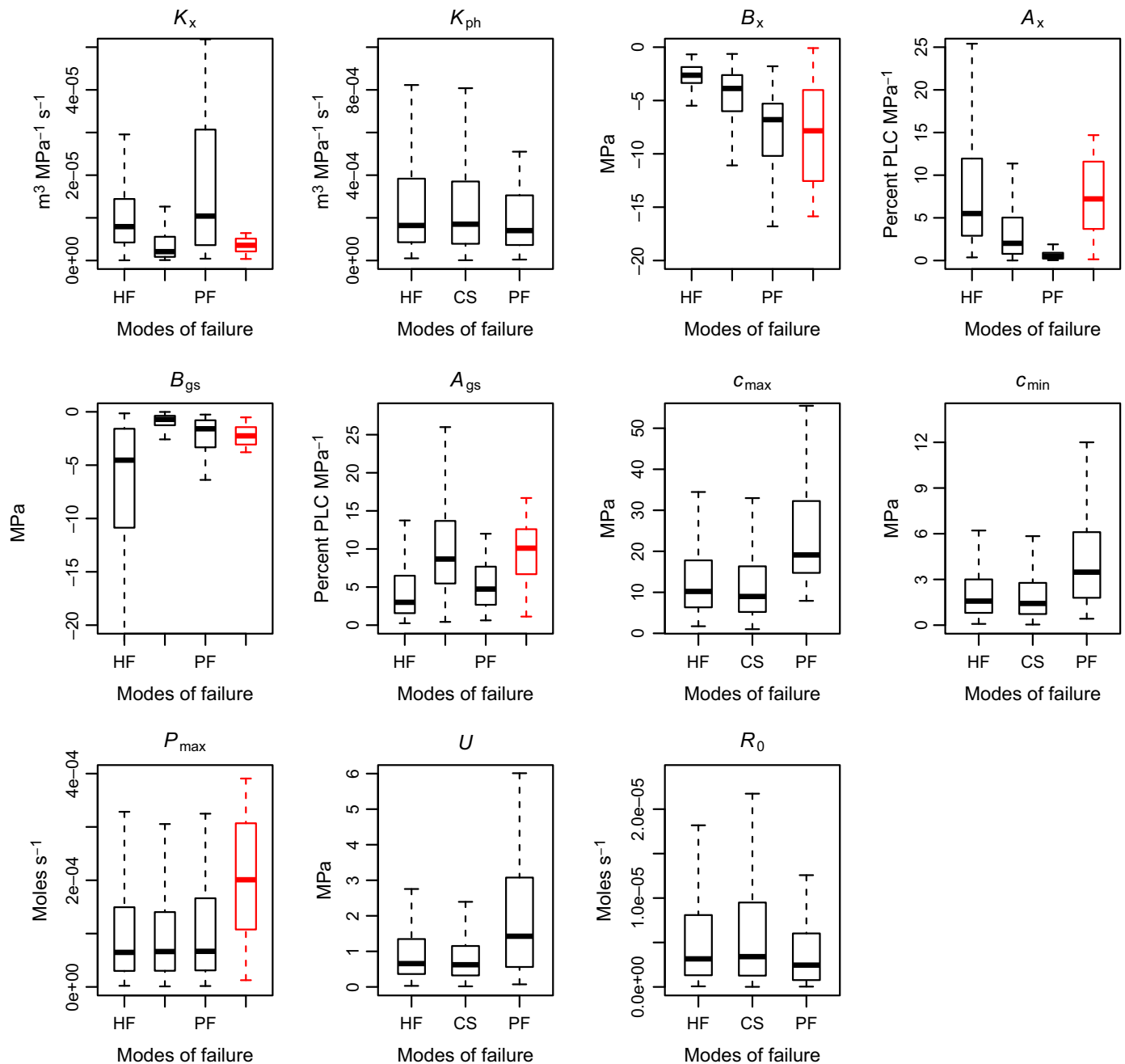


Fig. 2 Boxplot distribution of the 11 parameters varied in the model as a function of the three modes of failure (HF, hydraulic failure; CS, carbon starvation; PF, phloem transport failure). Boxplots provide mean and interquartile ranges for each parameter and each mode of failure. The first three boxes on the left in black give the modelled distributions, the last box on the right in red gives the distributions from the empirical data compilations, for those parameters for which empirical data were available. B_x , water potential Ψ causing 50% loss of K_{xyl} ; A_x , slope of the xylem vulnerability curve; c_{max} , leaf osmotic pressure at which P goes to zero; c_{min} , osmotic pressure above which R begins to increase as a function of c ; B_{gs} , water potential Ψ causing 50% decline in g_s ; A_{gs} , slope of the g_s curve as a function of water potential Ψ ; K_{ph} and K_x , phloem and xylem conductance, respectively; R_0 , base respiration rate; P_{max} , maximum photosynthesis; PLC, percentage loss of hydraulic conductivity; U , turgor pressure at the bottom of the phloem.

Discussion

Model structure and major assumptions

The model incorporates many of the interactions among the processes of carbohydrate fixation and transport and water transport and transpiration. By way of comparison, the Sperry *et al.* (1998)

model includes a very detailed representation of the linkage between gaseous and liquid water transport processes in the soil and the plant, but the processes linked to C fixation and transport are not represented (for an advanced combination of water- and C-related processes, see Mackay *et al.*, 2012). Conversely, models by Cannell & Thornley (2000) and Dewar (1993) represent C fixation and allocation using concepts related to source and sink

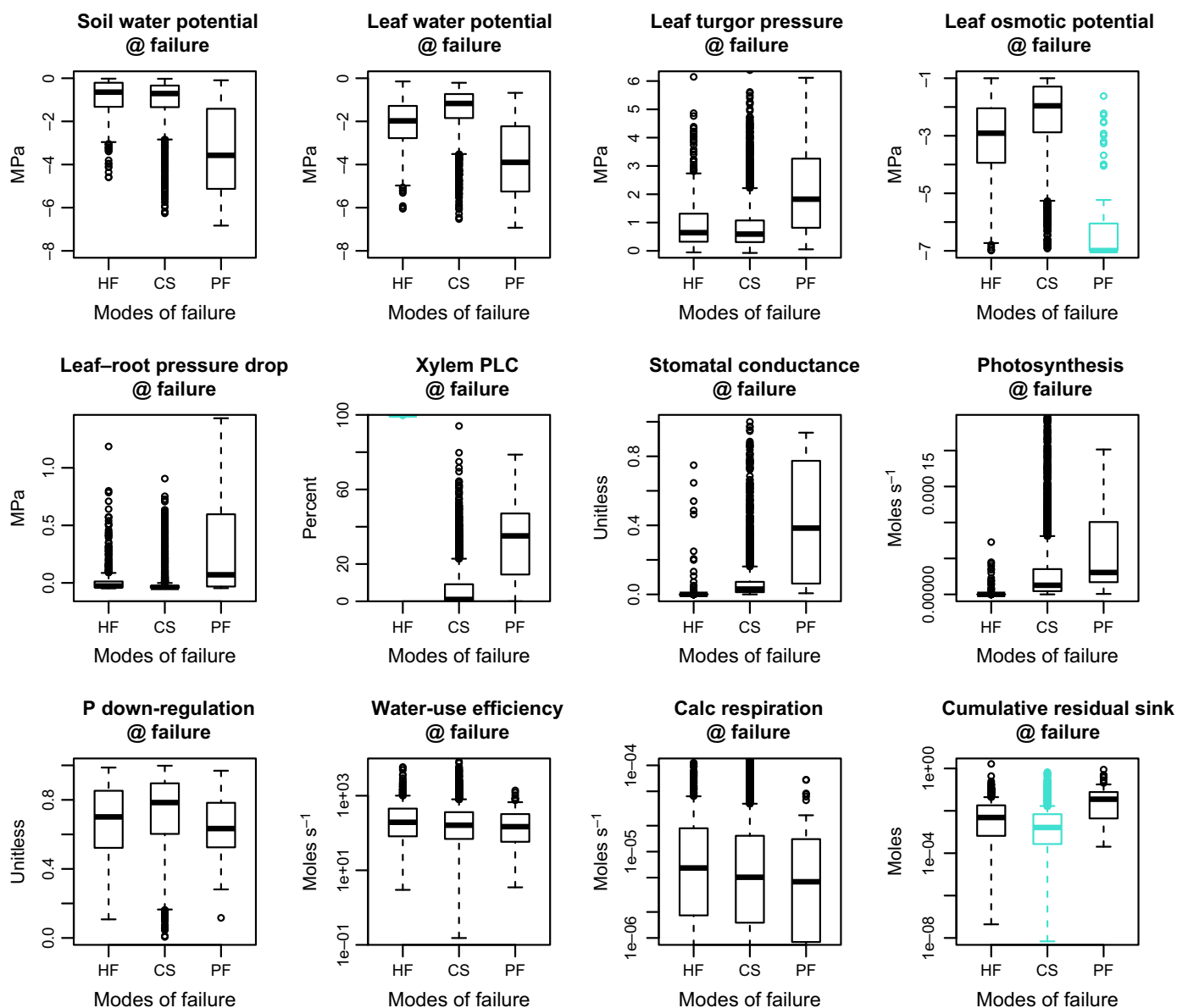


Fig. 3 Boxplot distribution of 12 variables calculated at the soil water potentials at which the plants failed, as a function of the three modes of failure (HF, hydraulic failure; CS, carbon starvation; PF, phloem transport failure). Boxplots provide mean and interquartile ranges for each variable and each mode of failure. For each of the three modes of failure, the variable most closely associated with that mode is shown in turquoise in the respective plot (i.e. leaf osmotic potential for PF; xylem percentage loss of hydraulic conductivity (PLC) for HF; residual flux (or cumulative stores) for CS). Note that the last three variables are plotted on a log scale.

strength, but the biophysical representation of xylem and phloem transport is missing. Finally, the model by De Schepper & Steppe (2010) is close to the approach presented here, but its focus is in simulating short-term (min to h) dynamics. The fundamental feature of this model is to include both stabilizing and destabilizing processes for xylem and phloem. In the case of phloem transport, the effect of viscosity on conductance is the main destabilizing process (Högltrå *et al.*, 2009a), viscosity being a strong nonlinear function of sucrose osmotic concentration (Morison, 2002).

We used a Bayesian approach based on literature information and expert knowledge to analyse parameter and model output distributions. In our case, limits to parameter distributions were

set using global compilations of parameter values. In addition, screening criteria were set to create boundaries for the parameter space ('behavioural' values). In Bayesian parlour, we constrained partially informative priors by logical criteria based on expert knowledge. Criterion (a) is well supported in the literature (Mencuccini, 2003; Martínez-Vilalta *et al.*, 2014). Criterion (b) is also regarded as a universal observation.

Coordination among modes of failure along water supply–demand axis

A plot of xylem vs stomatal P50 discriminated between HF and CS (McDowell *et al.*, 2008). The distribution of these two modes

Fig. 4 Distribution of the model simulations in the space defined by the xylem vulnerability to cavitation (P50) and the stomatal sensitivity to water potentials (stomatal P50) for the three main modes of failure (hydraulic failure, carbon starvation, phloem transport failure). For each panel, the colour scheme follows the leaf water potentials at failure (with warmer colours indicating more negative values), following the legend in the first panel.

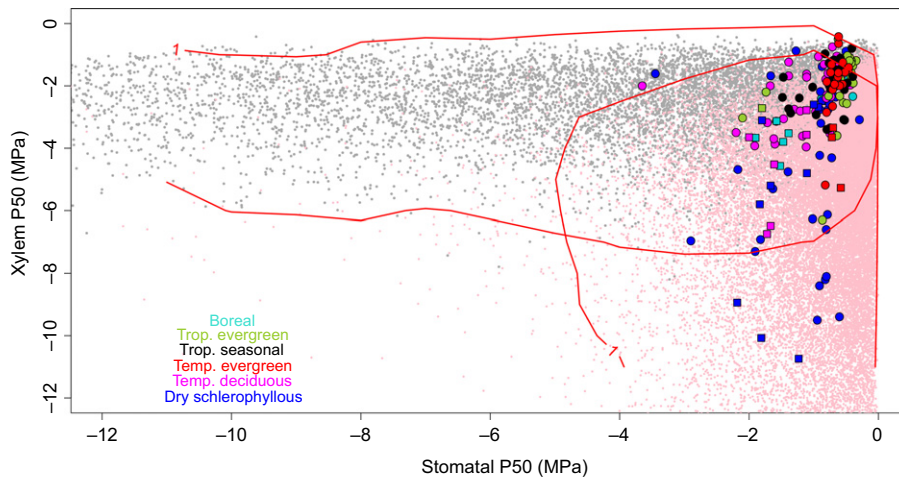
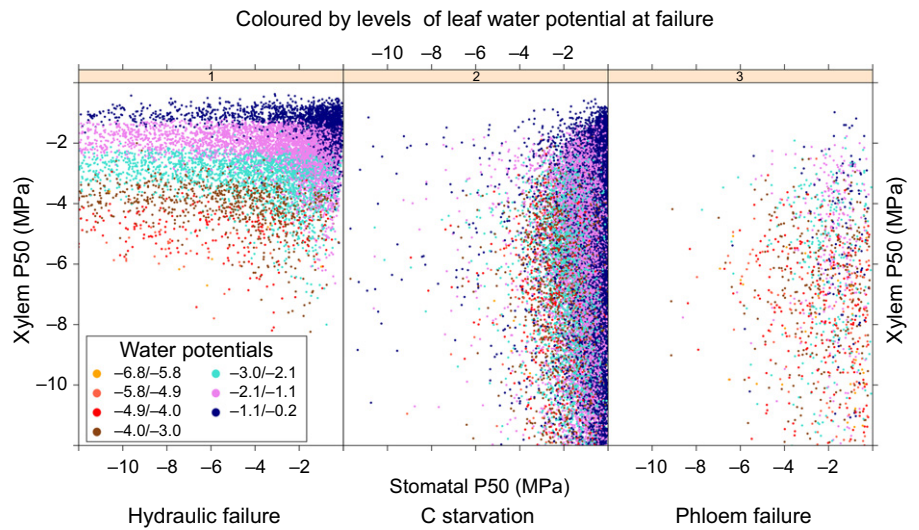


Fig. 5 Distribution of the model simulations in the space defined by xylem P50 and stomatal P50 as per Fig. 4. The two main modes of failure (hydraulic failure and carbon starvation) are highlighted with grey and pink points, respectively. Red contour lines indicate 99% relative densities of points for each distribution (e.g. < 1% of the grey points are located outside the corresponding thick red 1% contour). Red contour distributions are given separately for the grey points (hydraulic failure) and the pink points (carbon starvation). The area of joint occurrence of the two failure modes is therefore indicated by the intersection of the two 1% contour red lines. Biomes, turquoise, boreal; green, tropical evergreen; black, tropical seasonal; red, temperate evergreen; pink, temperate deciduous; blue, dry sclerophyllous. For each colour: circles, angiosperms; squares, gymnosperms.

Table 3 Results of the general linear model employed to explain xylem P50 as a function of stomatal P50, dataset, biome and plant group

	d.f.	Sum of squares	Mean square	F-value	Prob (> F)
Stomatal P50	1	114.482	114.48	80.79	9.24 e-16***
Dataset	5	214.34	42.87	30.25	< 2.2 e-16***
Biome	6	38.146	6.36	4.49	3.26 e-04***
Plant group	1	51.027	51.03	36.01	1.38 e-08***
Biome × plant group	4	53.692	13.42	9.47	7.28 e-07***
Residuals	152	215.384	1.42		

For the datasets based on estimates of turgor loss point (TLP), stomatal P50 was defined here as 70% of TLP (see text for further explanation and Supporting Information Tables S4, S5 for tests using different assumptions) ($n = 170$, $R^2_{adj} = 0.60$). ***, $P < 0.001$.

of failure is delimited by a diagonal space going from combinations of sensitive stomata plus vulnerable xylem to combinations of insensitive stomata and resistant xylem. Inside this diagonal space, both types of failure occurred. The significance of this diagonal space can be understood as follows. First, the variability in xylem conductance and stomatal conductance in relation to water and C fluxes depends on parameters that are, at least to some degree, correlated with one another (e.g. A_x , B_x with K_x and A_{gs} with B_{gs}). This reduces the dimensionality of the problem. Indeed, our sensitivity analysis (Table S2) showed that the failure mode was affected by a number of parameter combinations reflected in the covariances mentioned earlier. Second, one would expect that plants evolved strategies to minimize the relative risks caused by different mortality hazards. Traits that would cause plants to be situated entirely within the space of only one

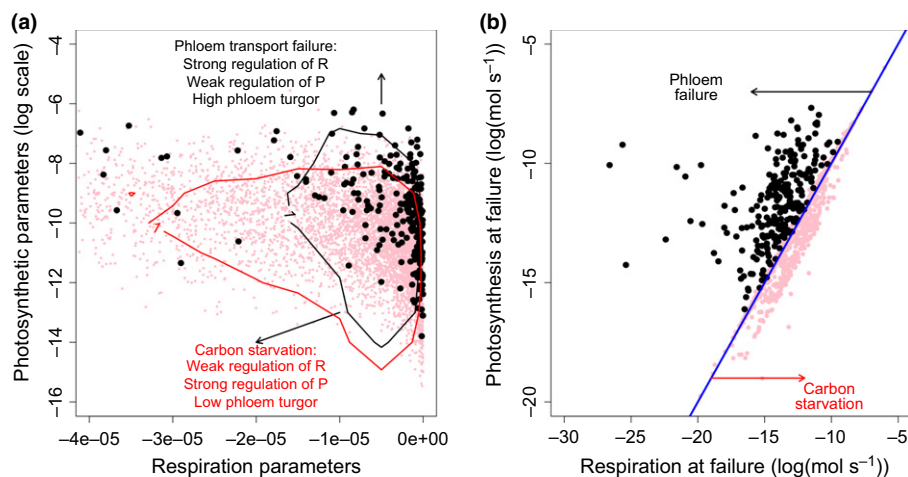


Fig. 6 (a) Distribution of the model simulations in the space defined by the combination of parameters controlling respiration vs those controlling photosynthesis. The pink points indicate the simulations resulting in carbon starvation (CS), while the black points indicate those resulting in phloem transport failure. Red and black contour lines indicate the respective 99% relative densities of points for each distribution, as per Fig. 5. The composite parameter controlling respiration is calculated as $(-R_0/U_{C_{min}})$. The composite parameter controlling photosynthesis is calculated as $P_{max} B_{gs}/c_{max}$. (b) The values of photosynthesis and respiration at failure are given for the runs resulting in CS (pink points) and phloem transport failure (black points). The blue line gives the 1 : 1 line of source–sink balance.

dominant hazard type would likely be evolutionary unstable. It is possible that different optimal solutions evolved such that different sets of functional traits lead to roughly equal chances of mortality by different processes. For example, PLC was $> 90\%$ for some of the simulations of CS (Fig. 3), while total cumulative F_{resid} were also comparatively higher for simulations of HF (Fig. 3). One may expect *a priori* that mortality be brought about by a coincidence of several different processes. Recent experiments directly testing mechanisms of mortality show that a single species can die by different causes depending on the circumstances (Sevanto *et al.*, 2014). It is interesting that the vast majority of the species for which empirical data were available were contained within this diagonal space (Fig. 5). This dataset of 170 species covered all major biomes, climate conditions and plant types (Table S1). The significant terms for ‘dataset’ found in the relationship between B_x and B_{gs} in the meta-analytical compilation suggests that caution is needed when different datasets are combined. However, when tested, we did not find a significant effect of the method employed to estimate B_{gs} (i.e. either from sap flow/conductance measurements or from Ψ_{dip}) based on three different tests. This finding supports the use of Ψ_{dip} as an indicator also of stomatal behaviour across species.

Coordination among modes of failure along carbon supply–demand axis

A plot of photosynthetic vs respiratory parameters discriminated combinations leading to CS from PF. Interestingly, many combinations could lead to both modes of failure. PF was associated with an altered balance between carbohydrate sources (less sensitively regulated in relation to drought) and sinks (more sensitively regulated) (Fig. 6). This altered balance produced larger residual carbohydrate fluxes and led to wider C safety margins

(*sensu* Mitchell *et al.*, 2014). These results suggest that plants in which growth continues at low water potentials may be more likely to suffer CS. Vice versa, plants may risk PF when consumption of carbohydrates responds sensitively while stomatal and photosynthetic rates remain high during drought. Interestingly, the proportion of combinations resulting in PF was strongly increased when a direct sink limitation by plant water status was introduced (Table S2).

Evidence for the response of photosynthetic nonstomatal parameters to drought was recently reviewed by Zhou *et al.* (2013). While growth is very sensitive to turgor reductions, the response of respiration to drought is more rarely documented. Duan *et al.* (2013, 2014) and Ayub *et al.* (2011) found that leaf dark respiration declined only at the end of severe droughts, while Metcalfe *et al.* (2010) reported increases in stem respiration during drought in a tropical rainforest. The response of growth to drought is almost never documented (for an exception, see Mitchell *et al.*, 2014).

The diagonal 1 : 1 line of Fig. 6(b) is the line of source–sink balance. CS and PF can both be avoided provided a plant can co-regulate source and sink activity with equal sensitivity during drought. This appears to be possible for some, but not all, parameter combinations (see the regions of overlap between the two failure modes in Fig. 6a). Combinations leading to HF were found well below the 1 : 1 source–sink balance line of Fig. 6(b), that is, in the same region as CS (data not shown). This is because hydraulic regulations of stomatal conductance during drought led to stomatal closure and lower photosynthesis, but not necessarily lower respiration rates. In our model, we assumed that photosynthesis and respiration, but not F_{resid} , were actively controlled by plant water status. In other words, the assumptions in our model are equivalent to the assumption that allocation to carbohydrate storage is a residual term.

It is important to note that CS was also affected by phloem properties, albeit indirectly, via the effects of changed phloem turgor, phloem osmotic potentials and phloem conductance. This is supported by the results of the sensitivity analyses of Tables S2 and S3. The osmotic and turgor variables at failure (leaf osmotic pressure at failure, leaf turgor pressure at failure) were affected by a combination of xylem, phloem and gas exchange parameters (Table S2).

Our steady-state model constrains the solutions to a space where turgor is kept constant, but phloem transport may also temporarily fail under dynamic conditions by reaching turgor loss for limited but crucial time periods (e.g. McDowell *et al.*, 2013; Sevanto *et al.*, 2014). For example, under drought, low photosynthesis may result in sucrose concentrations barely capable of maintaining a positive turgor pressure.

Nonsteady-state behaviour and timescales to mortality

How much would the conclusions drawn on the basis of Figs 5 and 6 change had we incorporated nonsteady state conditions? It is likely that additional failure modes exist that can only be identified under nonsteady-state conditions. However, the characterization of these additional modes is prevented by our lack of mechanistic understanding of the underlying processes. In addition, nonsteady-state models tend to be parameter-rich and their calibration within known uncertainty margins is difficult. Considering these limitations, a steady-state approach seems a reasonable first approximation. In the context of the variables studied here, the behaviour of a xylem hydraulic capacitor may primarily affect the magnitude of the declines in xylem water potentials, slowing down xylem cavitation and HF. For example, Meinzer *et al.* (2003) showed that diurnal changes in plant water potential and sap flow can be moderated significantly as a result of the presence of hydraulic capacitors, and cavitation of xylem conduits may have temporary moderating effects (see Hölttä *et al.*, 2009b). Alternatively, a leaf capacitor may primarily slow down the declines of water potential, thereby reducing stomatal closure and CS.

Dynamic carbohydrate storage under high photosynthetic rates may lower phloem loading and prevent excessive solute concentrations (and viscosity) in the phloem, but at the same time, carbohydrate release may prevent dangerously low sugar concentrations and loss of turgor under conditions of long and intense respiratory losses. Empirical data are currently unavailable to help tease out these possibilities.

Incorporating processes resulting in nonsteady-state conditions may be useful under significant hydraulic disequilibrium between soil and plant. Several causes of hydraulic disequilibrium have been reported (i.e. transient accumulation of solutes, lack of overnight equilibration in plant hydration, continued night-time transpiration; cf. Donovan *et al.*, 2003). Expanding this model to include processes occurring during longer time periods would allow probing of the significance of progressive leaf shedding, changing rooting depth and root:shoot ratios, xylem growth and refilling and cavitation fatigue.

Conclusions

The interpretation of mortality given here, of a process occurring along two independent axes representing the dimensions of water supply/demand and C supply/demand, differs significantly from McDowell *et al.* (2008), where the primary axis driving mortality was the degree of isohydric/anisohydric regulation of water potential. Stomatal behaviour turns out to be just one component of a strategy that minimizes the risk of three different modes of mortality. A plot of stomatal vs xylem P50 separated out the possible parameter combinations leading to HF from those leading to CS. Conversely, PF could be separated from CS by parameter combinations regulating phloem transport, respiration and photosynthesis. PF occurred especially when growth was assumed to respond sensitively to plant water status while stomatal regulation and photosynthetic down-regulation were limited. Maintaining phloem turgor via regulation of osmotic pressure, and the link between solute concentration and viscosity were crucial in understanding the relative sensitivity of growth and gas exchange to drought. With regard to model validation, this exercise showed that only about half of the parameters currently in the model could be constrained empirically. Some of the remaining parameters (i.e. sink turgor pressure) can be constrained using analogous leaf or root turgor measurements (M. Mencuccini *et al.*, unpublished); however, empirical calibration remains difficult for others (e.g. phloem-related parameters).

Acknowledgements

F.M. acknowledges support from the STReSS COST action (FP1106) for short-term scientific missions to Edinburgh and Barcelona. M.M. and Y.S. acknowledge support from NERC (project NE/IO107749/1). This research has been supported by the Spanish Ministry of Economy and Competitiveness through grant CGL2010-16373. We thank the ARC-NZ Vegetation Function Network for supporting the compilation of the Xylem Functional Traits dataset and Brendan Choat and Steven Jansen for granting us access to the data. We thank José Luis Ordóñez for assistance in the preparation of Fig. 1. The authors have no conflicts of interest to declare. The insights from five reviewers helped considerably to sharpen the focus of the analysis.

References

- Adams HD, Guardiola-Claramonte M, Barron-Gafford GA, Villegas JC, Breshers DD, Zou CB, Troch PA, Huxman TE. 2009. Temperature sensitivity to drought-induced tree mortality portends increased regional die-off under global-change-type drought. *Proceedings of the National Academy of Sciences, USA* 106: 7063–7066.
- Adams HD, Williams AP, Xu C, Rauscher SA, Jiang X, McDowell NG. 2013. Empirical and process-based approaches to climate-induced forest mortality models. *Frontiers in Plant Science* 4: 438.
- Allen CD, Macalady AK, Chenchouni H, Bachelet D, McDowell N, Vennetier M, Kitzberger T, Rigling A, Breshers DD, Hogg EH (Ted), *et al.* 2010. A global overview of drought and heat-induced tree mortality reveals emerging climate change risks for forests. *Forest Ecology and Management* 259: 660–684.

- Anderegg LDL, Anderegg WRL, Berry JA. 2013. Not all droughts are created equal: translating meteorological drought into woody plant mortality. *Tree Physiology* 33: 701–712.
- Anderegg WRL, Berry JA, Field CB. 2012. Linking definitions, mechanisms, and modeling of drought-induced tree death. *Trends in Plant Science* 17: 693–700.
- Ayub G, Smith RA, Tissue DT, Atkin OK. 2011. Impacts of drought on leaf respiration in darkness and light in *Eucalyptus saligna* exposed to industrial-age atmospheric CO₂ and growth temperature. *New Phytologist* 190: 1003–1018.
- Bancal P, Soltani F. 2002. Source–sink partitioning. Do we need Münch? *Journal of Experimental Botany* 53: 1919–1928.
- Bartlett MK, Scoffoni C, Sack L. 2012. The determinants of leaf turgor loss point and prediction of drought tolerance of species and biomes: a global meta-analysis. *Ecology Letters* 15: 393–405.
- Bijlsma RJ, Lambers H. 2000. A dynamic whole-plant model of integrated metabolism of nitrogen and carbon. 2. Balanced growth driven by C fluxes and regulated by signals from C and N substrate. *Plant and Soil* 220: 71–87.
- Beven KJ, Binley AM. 1992. The future of distributed models: model calibration and uncertainty prediction. *Hydrological Processes* 6: 279–298.
- Cannell MGR, Thornley JHM. 2000. Modelling the components of plant respiration: some guiding principles. *Annals of Botany* 85: 45–54.
- Choat B, Jansen S, Brodribb TJ, Cochard H, Delzon S, Bhaskar R, Bucci SJ, Field TS, Gleason SM, Hacke UG *et al.* 2012. Global convergence in the vulnerability of forests to drought. *Nature* 491: 752–756.
- Cochard H. 2006. Cavitation in trees. *Comptes Rendus Physique* 7: 1018–1126.
- Dewar R. 1993. A root–shoot partitioning model based on carbon–nitrogen–water interactions and Münch phloem flow. *Functional Ecology* 7: 356–368.
- Dobbertin M, Rigling A. 2006. Pine mistletoe (*Viscum album ssp. austriacum*) contributes to Scots pine (*Pinus sylvestris*) mortality in the Rhone valley of Switzerland. *Forest Pathology* 36: 309–322.
- Donovan LA, Richards JH, Linton MJ. 2003. Magnitude and mechanisms of disequilibrium between predawn plant and soil water potentials. *Ecology* 84: 463–470.
- Duan H, Amthor JS, Duursma RA, O’Grady AP, Choat B, Tissue DT. 2013. Carbon dynamics of eucalypt seedlings exposed to progressive drought in elevated [CO₂] and elevated temperature. *Tree Physiology* 33: 779–792.
- Duan H, Duursma RA, Huang G, Smith RA, Choat B, O’Grady AP, Tissue DT. 2014. Elevated [CO₂] does not ameliorate the negative effects of elevated temperature on drought-induced mortality in *Eucalyptus radiata* seedlings. *Plant, Cell & Environment* 37: 1598–1613.
- Farrar J. 1996. Regulation of root weight ratio is mediated by sucrose: opinion. *Plant and Soil* 185: 13–19.
- Fisher R, McDowell NG, Purves D, Moorcroft P, Sitch S, Cox P, Huntingford C, Meit P, Woodward FIW. 2010. Assessing uncertainties in a second-generation dynamic vegetation model caused by ecological scale limitations. *New Phytologist* 187: 666–681.
- Galiano L, Martínez-Vilalta J, Lloret F. 2011. Carbon reserves and canopy defoliation determine the recovery of Scots pine 4 yr after a drought episode. *New Phytologist* 190: 750–759.
- Hair JF Jr, Anderson RE, Tatham RL, Black WC. 1998. *Multivariate data analysis*, 5th edn. London, UK: Prentice Hall Inc.
- Hartmann H, Trumbore S, Ziegler W. 2013. Lethal drought leads to reduction in nonstructural carbohydrates (NSC) in Norway spruce tree roots but not in the canopy. *Functional Ecology* 27: 413–427.
- Heiniger U, Theile F, Rigling A, Rigling D. 2011. Blue stain infections in roots, stems and branches of declining *Pinus sylvestris* trees in a dry inner alpine valley in Switzerland. *Forest Pathology* 41: 501–509.
- Hölttä T, Mencuccini M, Nikinmaa E. 2009a. Linking phloem function to structure: analysis with a coupled xylem–phloem transport model. *Journal of Theoretical Biology* 259: 325–337.
- Hölttä T, Mencuccini M, Nikinmaa E. 2009b. Capacitive effects of cavitation in xylem conduits: results from a dynamic model. *Plant, Cell & Environment* 32: 10–21.
- Jarvis PG, McNaughton KG. 1986. Stomatal control of transpiration: scaling up from leaf to region. *Advances in Ecological Research* 15: 1–49.
- Jensen KH, Savage JA, Holbrook NM. 2013. Optimal concentration for sugar transport in plants. *Journal of the Royal Society Interface* 10: doi: 10.1098/rsif.2013.0055.
- Klein T. 2014. The variability of stomatal sensitivity to leaf water potential across tree species indicates a continuum between isohydric and anisohydric behaviours. *Functional Ecology* 28: 1313–1320.
- Krams I, Daukste J, Kivleniece I, Brumelis G, Cibulskis R, Āboliņš-Ābols M, Rantala MJ, Mierauskas P, Krama T. 2012. Drought-induced positive feedback in xylophagous insects: easier invasion of Scots pine leading to greater investment in immunity of emerging individuals. *Forest Ecology and Management* 270: 147–152.
- Lang A. 1978. A model of mass flow in the phloem. *Australian Journal of Plant Physiology* 5: 535–546.
- Mäkelä A, Berninger F, Hari P. 1996. Optimal control of gas exchange during drought: theoretical analyses. *Annals of Botany* 77: 461–467.
- Mackay DS, Ewers BE, Loranty MM, Kruger EL, Samanta S. 2012. Bayesian analysis of canopy transpiration models: a test of posterior parameter means against measurements. *Journal of Hydrology* 432–433: 75–83.
- Manzoni S, Vico G, Katul G, Porporato A. 2013. Biological constraints on water transport in the soil–plant–atmosphere system. *Advances in Water Resources* 51: 292–304.
- Manzoni S, Vico G, Katul G, Palmroth S, Porporato A. 2014. Optimal plant water-use strategies under stochastic rainfall. *Advances in Water Resources* 50: 5379–5394.
- Martínez-Vilalta J, Poyatos R, Aguadé D, Retana J, Mencuccini M. 2014. A new look at water transport regulation in plants. *New Phytologist* 204: 105–115.
- McDowell NG, Pockman W, Allen C, Breshears D, Cobb N, Kolb T, Plaut J, Sperry J, West A, Williams D *et al.* 2008. Mechanisms of plant survival and mortality during drought: why do some plants survive while others succumb? *New Phytologist* 178: 719–739.
- McDowell NG, Sevanto S. 2010. The mechanisms of CS: how, when, or does it even occur at all? *New Phytologist* 186: 264–266.
- McDowell NG. 2011. Mechanisms linking drought, hydraulics, carbon metabolism, and vegetation mortality. *Plant Physiology* 155: 1051–1059.
- McDowell NG, Fisher R, Xu C, Domec JC, Hölttä T, Mackay DS, Sperry JS, Boutz A, Dickman L, Gehres N *et al.* 2013. Evaluating theories of drought-induced vegetation mortality using a multimodel–experiment framework. *New Phytologist* 200: 304–321.
- Meinzer FC, James SA, Goldstein G, Woodruff D. 2003. Whole-tree water transport scales with sapwood capacitance in tropical forest canopy trees. *Plant, Cell & Environment* 26: 1147–1155.
- Meir P, Mencuccini M, Dewar R. 2015. Drought-related tree mortality: addressing the gaps in understanding and prediction. *New Phytologist* 207: 28–33.
- Mencuccini M. 2003. The ecological significance of long distance water transport: short-term regulation and long-term acclimation across plant growth forms. *Plant, Cell & Environment* 26: 163–182.
- Metcalfe DB, Meir P, Aragão LEOC, Lobo-do-Vale R, Galbraith D, Fisher RA, Chaves MM, Maroco JP, da Costa ACL, de Almeida SS *et al.* 2010. Shifts in plant respiration and carbon use efficiency at a large-scale drought experiment in the eastern Amazon. *New Phytologist* 187: 608–621.
- Minchin PEH, Thorpe MR, Farrar JF. 1993. A simple mechanistic model of phloem transport which explains sink priority. *Journal of Experimental Botany* 44: 947–955.
- Minchin PEH, Thorpe MR. 1996. What determines carbon partitioning between competing sinks? *Journal of Experimental Botany*, 47(Special Issue): 1293–1296.
- Minunno F, van Oijen M, Cameron DR, Pereira JS. 2013. Selecting parameters for Bayesian calibration of a process-based model: a methodology based on canonical correlation analysis. *Journal on Uncertainty Quantification* 1: 370–385.
- Mitchell PJ, O’Grady AP, Tissue DT, White DA, Ottenschlaeger ML, Pinkard EA. 2013. Drought response strategies define the relative contributions of hydraulic dysfunction and carbohydrate depletion during tree mortality. *New Phytologist* 197: 862–872.

- Mitchell PJ, O'Grady AP, Tissue DT, Worledge D, Pinkard EA. 2014. Co-ordination of growth, gas exchange and hydraulics define the carbon safety margin in tree species with contrasting drought strategies. *Tree Physiology* **34**: 443–458.
- Morison KR. 2002. Viscosity equations for sucrose solutions: old and new. In: *Green processing and sustainability. Proceedings of APCCbE Conference and CHEMECA 2002*, 29 Sep–3 Oct 2002, Christchurch, New Zealand: Paper no. 984.
- Nardini A, Luglio J. 2014. Leaf hydraulic capacity and drought vulnerability: possible trade-offs and correlations with climate across three major biomes. *Functional Ecology* **28**: 810–818.
- Pammenter NW, Vander Willigen C. 1998. A mathematical and statistical analysis of the curves illustrating vulnerability of xylem to cavitation. *Tree Physiology* **18**: 589–593.
- Paul MJ, Foyer CH. 2001. Sink regulation of photosynthesis. *Journal of Experimental Botany* **52**: 1383–1400.
- Peng C, Ma Z, Lei X, Zhu Q, Chen H, Wang W, Liu S, Li W, Fang X, Zhou X. 2011. A drought-induced pervasive increase in tree mortality across Canada's boreal forests. *Nature Climate Change* **1**: 467–471.
- Poyatos R, Aguadé D, Galiano L, Mencuccini M, Martínez-Vilalta J. 2013. Drought-induced defoliation and long periods of near-zero gas exchange play a key role in accentuating metabolic decline of Scots pine. *New Phytologist* **200**: 388–401.
- Powell TL, Galbraith DR, Christoffersen BO, Harper A, Imbuzeiro HMA, Rowland L, Almeida S, Brando PM, da Costa ACL, Costa MH *et al.* 2013. Confronting model predictions of carbon fluxes with measurements of Amazon forests subjected to experimental drought. *New Phytologist* **200**: 350–365.
- R Development Core Team (2013) *R: a language and environment for statistical computing*. Vienna, Austria: R Foundation for Statistical Computing. URL <http://www.R-project.org/>.
- Sala A. 2009. Lack of direct evidence for the carbon-starvation hypothesis to explain drought induced mortality in trees. *Proceedings of the National Academy of Sciences, USA* **106**: E68.
- Sala A, Piper F, Hoch G. 2010. Physiological mechanisms of drought-induced tree mortality are far from being resolved. *New Phytologist* **186**: 274–281.
- De Schepper V, Steppe K. 2010. Development and verification of a water and sugar transport model using measured stem diameter variations. *Journal of Experimental Botany* **61**: 2083–2099.
- Sevanto S, McDowell NG, Dickman LT, Pangle R, Pockman WT. 2014. How do trees die? A test of the hydraulic failure and carbon starvation hypotheses. *Plant, Cell & Environment* **37**: 153–161.
- Sperry JS, Adler FR, Campbell GS, Comstock JP. 1998. Limitation of plant water use by rhizosphere and xylem conductance: results from a model. *Plant, Cell & Environment* **21**: 347–359.
- Thornley JHM, Johnson IR. 1990. *Plant and crop modelling: a mathematical approach to plant and crop physiology*. Oxford, UK: Clarendon Press.
- Tuzet A, Perrier A, Leuning R. 2003. A coupled model of stomatal conductance, photosynthesis and transpiration. *Plant, Cell & Environment* **7**: 1097–1116.
- van Oijen M, Reyer C, Bohn FJ, Cameron DR, Deckmyn G, Flechsig M, Härkönen S, Hartig F, Huth A, Kiviste A *et al.* 2013. Bayesian calibration, comparison and averaging of six forest models, using data from Scots pine stands across Europe. *Forest Ecology and Management* **289**: 255–268.
- von Caemmerer S, Farquhar GD. 1981. Some relationships between the biochemistry of photosynthesis and the gas exchange of leaves. *Planta* **153**: 376–387.
- Venables WN, Ripley BD. 2002. *Modern applied statistics with S, 4th edn*. New York, NY, USA: Springer.
- Vilagrosa A, Hernandez EI, Luis VC, Cochard H, Pausas JG. 2014. Physiological differences explain the co-existence of different regeneration strategies in Mediterranean ecosystems. *New Phytologist* **201**: 1277–1288.
- Xu C, McDowell NG, Sevanto S, Fisher RA. 2013. Our limited ability to predict vegetation mortality. *New Phytologist* **200**: 298–300.
- Wermelinger B, Rigling A, Schneider Mathis D, Dobberrin M. 2008. Assessing the role of bark- and wood-boring insects in the decline of Scots pine (*Pinus sylvestris*) in the Swiss Rhone valley. *Ecological Entomology* **33**: 239–249.
- Wright IJ, Reich PB, Cornelissen JHC, Falster DS, Garnier E, Hikosaka K, Lamont BB, Lee W, Oleksyn J, Osada N *et al.* 2005. Assessing the generality of global leaf trait relationships. *New Phytologist* **166**: 485–496.
- Zhou S, Duursma RA, Medlyn BE, Kelly JW, Prentice IC. 2013. How should we model plant responses to drought? An analysis of stomatal and non-stomatal responses to water stress. *Agricultural and Forest Meteorology* **182–183**: 204–214.
- Zweifel R, Bangerter S, Rigling A, Sterck FJ. 2012. Pine and mistletoes: how to live with a leak in the water flow and storage system? *Journal of Experimental Botany* **63**: 2565–2578.

Supporting Information

Additional supporting information may be found in the online version of this article.

Fig. S1 Illustration of the theoretical relationships used in the model.

Fig. S2 Distribution of observations of xylem and stomatal P50, when stomatal P50 is defined as 100% of measured TLP.

Fig. S3 Distribution of observations of xylem and stomatal P50, when stomatal P50 is defined as 30% of measured TLP.

Table S1 Compilation of datasets of plant hydraulic traits by biome or plant functional types

Table S2 Results of the model sensitivity analysis carried out by means of a canonical correlation analysis

Table S3 Sensitivity analysis of frequency distribution of failure modes

Table S4 Stomatal P50 defined as 30% of TLP

Table S5 Stomatal P50 defined as 100% of TLP

Notes S1 Sensitivity analysis of model outputs in relation to inputs.

Notes S2 Sensitivity analysis of definition of leaf turgor loss point (TLP) as point of stomatal P50.

Please note: Wiley Blackwell are not responsible for the content or functionality of any supporting information supplied by the authors. Any queries (other than missing material) should be directed to the *New Phytologist* Central Office.